Atmos. Chem. Phys. Discuss., 12, 4541–4588, 2012
www.atmos-chem-phys-discuss.net/12/4541/2012/
doi:10.5194/acpd-12-4541-2012

Atmospheric Chemistry and Physics Discussions

Anthropogenic and forest fire pollution aerosol transported to the Arctic: observations from the POLARCAT-France spring campaign

B. Quennehen[1,4], A. Schwarzenboeck[1], A. Matsuki[2], J. F. Burkhart[3], A. Stohl[3], G. Ancellet[4], and K. S. Law[4]

[1]Laboratoire de Météorologie Physique, Université Blaise Pascal, CNRS/INSU, UMR6016, Aubière, France
[2]Frontier Science Organization, Kanazawa University, Japan
[3]Norwegian Institute for Air Reasearch (NILU), Kjeller, Norway
[4]UPMC Univ. Paris 06, Université Versailles St-Quentin, CNRS/INSU, LATMOS-IPSL, UMR8190, Paris, France

Received: 23 January 2012 – Accepted: 30 January 2012 – Published: 8 February 2012

Correspondence to: B. Quennehen (quennehen@latmos.ipsl.fr)

Published by Copernicus Publications on behalf of the European Geosciences Union.

Abstract

During the POLARCAT-France airborne measurement campaign in spring 2008, several pollution plumes transported from mid-latitude regions were encountered. The study presented here focuses on air masses from two different geographic origins (Europe and Asia) and from 2 different source types (anthropogenic pollution and forest fires). One case study analyses an European air mass, which was sampled during three consecutive day. Modelling of the aerosol particle ageing by coagulation suggests that coagulation cannot solely explain the evolution of the size distributions, which is particularly true for the accumulation mode. Analyses of the aerosol refractory size distributions indicate that the Aitken mode was mostly composed of volatile compounds, while accumulation mode particles desorbed to a refractory mode yielding a modal mean diameter evolving from 48 to 59 nm for the three consecutive days of sampling the same air mass. The single refractory mode suggests an internally mixed aerosol population which is supported from electron microscopy and subsequent EDX analyses of the accumulation mode particles.

Another case study focuses on European air masses polluted by fire emissions and Asian air masses with contributions from both biomass burning and anthropogenic emissions. On the one hand, the aerosol size distributions of the European biomass burning plumes are almost mono-modal with most of the particles found in the aged accumulation mode which desorbed uniformly. On the other hand, Asian air masses were more complex because of the mixing of different source contributions related to more variable and multimodal ambient and refractory aerosol size distributions. Electron microscopy illustrated soot-like inclusions in several samples. Within samples attributed to forest fire sources, the chemical signature is highly associated with the presence of potassium, which is characteristic for biomass burning plumes. The particle images suggest an internal mixing of sampled aerosol particles.

ACPD
12, 4541–4588, 2012

1 Introduction

Since the polar regions are more sensitive to global change than others (IPCC, 2007), a better understanding of the polar climate system is fundamental. This is why an increasing number of studies in the Arctic are dedicated to the collection of measurement data in order to improve our current understanding on climate related processes in the Arctic atmosphere (Law and Stohl, 2007). While ground based observations have been regularly performed at a few existing measurement stations (e.g. Sharma et al., 2002, 2004, 2006 and Quinn et al., 2002, 2007), aircraft observations of the Arctic atmosphere remain rare.

Aerosol particles play an important role in the global climate (IPCC, 2007) through their direct (McCormick and Ludwig, 1967) and indirect effects (Twomey, 1977; Albrecht, 1989) on Earth's radiative budget. These effects remain poorly investigated in the Arctic regions and are difficult to quantify, implicating large uncertainties (Garrett and Zhao, 2006; Lubin and Vogelmann, 2006). Since few pollution sources exist in the Arctic regions (e.g. the Kola peninsula as shown by Frossard et al., 2011 and Merlaud et al., 2011), polluted air masses observed in the Arctic are mainly transported from mid-latitude regions, leading for example to the build up of Arctic Haze, firstly observed by pilots flying over Arctic regions (Greenaway, 1950; Mitchell, 1957), more recently the phenomenon has been discussed with respect to its spatial extent by Dreiling and Friederich (1997), and summarised by Quinn et al. (2007). Arctic haze studies were mainly conducted to investigate the chemical and optical properties of Arctic Haze aerosol particles (Schnell, 1984; Clarke et al., 1984; Brock et al., 1990). Arctic Haze is mainly composed of particulate organic matter and sulphate and, to a lower extent, black carbon (Quinn et al., 2002). It originates from biomass burning and/or anthropogenic sources from any continent in the Northern Hemisphere. Eurasia (including Europe, former USSR countries, Siberia and Northern China) is considered to be the major source region for Arctic Haze, particularly observed during the winter and early spring seasons (Stohl, 2006; Sharma et al., 2004, 2006; Hirdman et al., 2010; Huang et al., 2010; Brock et al., 2011).

ACPD
12, 4541–4588, 2012

However, aerosol characteristics in the Arctic are different from what they are in the source regions. This is due to ageing and/or removal processes which occur on the pathway of the pollution plume from its sources to the Arctic. The principal transformation processes are listed below:

- Coagulation: this is the process of a particle to colliding with another one, thus forming one larger particle. As a consequence coagulation is reducing the total particle number concentration at a rate proportional to the square of particle concentration (Hinds, 1999).
- Condensation: this process corresponds to the growth of particles by condensation of the gas phase on particles (Hinds, 1999). Main condensable gases are depending on the pollution sources.
- Cloud processing: a part of the aerosol population is activated as cloud condensation nuclei and subsequently chemically transformed in the liquid phase (Seinfeld and Pandis, 1998).
- Dilution: by mixing surrounding air into a highly concentrated pollution plume, aerosol mass concentrations are reduced.

In addition, during their lifecycle, aerosols are subject to various removal processes:

- Dry deposition, which is most efficient for coarse mode particles (Seinfeld and Pandis, 1998).
- Wet deposition, which affects mostly accumulation mode particles. It corresponds to the in-cloud scavenging (washout) and below-cloud scavenging (rainout) (Seinfeld and Pandis, 1998).

In this context, and within the frame of the 4th International Polar Year (IPY, 2007–2008), the POLARCAT (POLar study using Aircraft, Remote sensing, surface measurements and models, of Climate, chemistry, Aerosols and Transport) project was

ACPD
12, 4541–4588, 2012

launched. The objectives within POLARCAT are particularly focusing on improving our knowledge related to long-range transport of short-lived pollutants (particulates and gases) to the Arctic. The approach chosen for POLARCAT has been to combine aircraft (in-situ and remote-sensing) measurements with extensive model studies. Within the French contribution to the POLARCAT project, the French ATR-42 research aircraft was deployed out of Kiruna, Sweden in April 2008 and out of Kangerlussuaq, Greenland in July 2008. It performed 24 scientific flights with state of the art instrumentation measuring physical and optical aerosol properties. While for the summer campaign, studies have been presented recently (Schmale et al., 2011; Quennehen et al., 2011), this work focuses on the spring aerosol measurements. Most recently, Adam de Villiers et al. (2010) and Merlaud et al. (2011) prsented results from the spring measurements of aerosol optical properties and NO_2 chemistry, respectively.

The main objective of the study presented here is to investigate the physical properties of pollution aerosol particles transported to the Arctic demonstrating particularly aerosol ageing observed from measurement data during the campaign. In the following, after a short presentation of the measurement instrumentation, the paper is focusing on two case studies, presented in separate sections three and four. The first case study is related to an European anthropogenic polluted air mass sampled during three consecutive days, in order to study transformation of aerosol particles within pollution plumes transported to the Arctic. The transformation is particularly seen in the Aitken mode. The second case study focuses on Eurasian polluted air masses, including Russian and Siberian forest fires, as well as an Asian anthropogenic plume.

ACPD
12, 4541–4588, 2012

2 Instrumentation on board the ATR-42 French aircraft and analysis of air mass origins

2.1 Instrumentation

2.1.1 Aerosol physical properties

Since the POLARCAT spring campaign was dedicated to cloud studies, a CVI (Counterflow Virtual Impactor, Schwarzenboeck et al., 2000) inlet was operated on the ATR-42. The CVI inlet is equipped with a backward facing interstitial inlet and can also be operated isokinetically for total aerosol sampling in clear sky conditions. For isokinetic sampling, the counterflow was switched off, and the controlled flow is increased to meet measured air speed in the shroud. Downstream the inlet, clear sky aerosol size distributions were measured by the combination of a Scanning Mobility Particle Sizer (SMPS, Villani et al., 2008) and an Optical Particle Counter (OPC, Grimm model 1.108), both operated inside the ATR-42 cabin. While the SMPS measured particle number size distributions in the range $20 < D_p < 500$ nm, where D_p is the particle diameter, the OPC sized particles with diameters in the range $300 < D_p < 2000$ nm. The number concentrations derived from SMPS plus OPC are compared with total concentration from a Condensation Particle Counter (CPC 3010, TSI), which measured particles with diameter greater than 10 nm.

In addition, the aerosol particle volatility was measured with a second set of SMPS and OPC instruments heated up to 280 °C using a thermo-denuder located upstream the second set of SMPS and OPC. After the thermal conditioning, refractory particles are supposed to be mainly composed of soot, sea salt, mineral dust and some refractory fraction of organic carbon. Ambient and 280 °C particle volume concentrations were calculated and used in order to determine the aerosol volatile fraction:

$$F_{\text{volatile}} = \frac{V_{\text{ambient}} - V_{280\,^\circ\text{C}}}{V_{\text{ambient}}} \quad (1)$$

ACPD
12, 4541–4588, 2012

$F_{volatile}$ represents the volume fraction of particulate matter volatilised after heating. The volatile volume fraction of solely accumulation mode particles $F_{volatile,ac}$ is calculated in the following way:

$$F_{volatile,ac} = \frac{V_{ambient,ac} - V_{280\,°C,ac(ref)}}{V_{ambient,ac}} \quad (2)$$

where $V_{ambient,ac}$ is the aerosol accumulation mode volume and $V_{280\,°C,ac(ref)}$ is the volume of the refractory accumulation mode. Finally, the number fraction of solely accumulation mode volatile particles ($F_{conc,ac}$) is calculated acccordingly:

$$F_{conc,ac} = \frac{N_{280\,°C,ac(ref)}}{N_{ambient,ac}} \quad (3)$$

with $N_{ambient,ac}$ and $N_{280\,°C,ac(ref)}$ corresponding to the aerosol accumulation mode concentration at ambient temperature and at 280 °C, respectively. The measurement efficiencies of both SMPS/OPC systems were inter-compared regularly during the campaign, usually before take-off and without thermo-desorption. Deviations between both systems were found to be below the instrument uncertainties (Quennehen et al., 2011).

2.1.2 Aerosol optical properties

In addition to the physical and chemical aerosol properties, the aerosol light absorption coefficient has been measured with a Particle Soot Absorption Photometer (PSAP, Bond et al., 1999). Its detection limit is 1 Mm^{-1} which can be reduced by temporal averaging using the method described by Springston and Sedlacek (2007). In our study the transmission efficiency has been processed with a running average over 180 leading to a decreased detection limit of 0.17 Mm^{-1}.

2.1.3 Aerosol chemical properties and trace gas concentrations

The chemical composition of aerosol particles was investigated using aerosol samples collected by a two-stage impactor. The impactor type used in this study is identical to

ACPD
12, 4541–4588, 2012

that described in Matsuki et al. (2005a,b). The 50 % cut-off aerodynamic diameters are 1.6 and 0.2 µm for the first and second stage, respectively with a volume flow rate of approximately 1.0 l min^{-1} (1013 hPa, 293 K). Thus, in practice, supermicron particles are found in the first stage of the impactor while submicron particles impact during the second stage. The aim of the individual particle analysis within the spring campaign was to study both pollution aerosol particles from clear sky samples and residual particles from liquid/ice phase Arctic cloud samples. The frequency and duration of the individual samples taken during the flights were a function of the flight patterns and spatial extent of pollution plumes/cloud samplings during respective flights. More information about the sampling substrate of the impactor is given in Matsuki et al. (2010).

In-situ samples were then analysed in the laboratory after the flights. Submicron samples were imaged utilising a transmission electron microscope (TEM, JEM-2010FEF, JEOL) to obtain high resolution images. Furthermore, an Energy Dispersion X-ray spectrometer (EDX, JED-2300, JEOL) monitored X-ray spectra to obtain elemental composition of individual particles. Supermicron particles were analysed by a Scanning Electron Microscope (SEM, S-3000N, Hitachi) coupled to an other EDX (EMAX-500, Horiba). The relative atomic ratios (%) of the detected elements were quantified by the manufacturer's software in standard-less mode. Due to the limitation of the method related to the quantification of lighter elements contained in a single particle, C, N, and O were excluded from the quantitative analysis. For each sample of the submicron particles, 30 randomly chosen particles were analysed while for supermicron samples, every single particle was analysed. The number of analysed supermicron particles ranged from 16 to more than 50, depending on the particle loading of individual filters.

Carbon monoxide (CO, also investigated by Adam de Villiers et al., 2010) trace gas was measured by the MOZART CO instrument, based on the gas filtered correlation principle of infrared absorption by the 4.67 µm fundamental vibration-rotation band of CO (Nédélec et al., 2003). CO is a rather inert tracer over a timescale of 10–20 days and is emitted by combustion processes (both biomass burning and anthropogenic combustion, Forster et al., 2001). Additionally, NO_2 measurements were performed

ACPD
12, 4541–4588, 2012

using an Airbone Limb Scanning – Differential Optical Absorption Spectrometer (ALS-DOAS) as presented in Merlaud et al. (2011).

2.2 Air mass origins and ages

In order to derive the origins of air masses sampled during the POLARCAT-France spring campaign, the FLEXPART Lagrangian particle dispersion model (version 6.2) (Stohl et al., 1998, 2005) was used in its backward mode (Stohl et al., 2003). The model was repeatedly initialised along the flight trajectories for aircraft position changes of more than 0.20° in horizontal dimension and/or 150 m in vertical dimension. For every single run, 40 000 particles were released from a small volume around the aircraft position and then were tracked during twenty days (backwards in time). The primary output of FLEXPART backward calculations is the potential emission sensitivity (PES), column-integrated values of which were used here mainly to characterise the origin and transport pathways of the sampled air masses. Footprint potential emission sensitivities (FPES) correspond to the PES values of the lowest layer in the model output (0–100 m). Since pollutant emissions mostly occur at the Earth's surface, FPES provide important information about the potential sources of pollution for the sampled air masses. In addition to PES and FPES, hot spots detected by the radiospectrometer MODIS (Giglio et al., 2003) are indicated in red and black illustrating forest fires and other fires (e.g. agricultural), respectively.

FLEXPART also processes information about calculated time for every released single particle to reach the ground (source). The information about residence times (in the air) of single particles then leads to an age spectrum ranging from one to twenty days. For a specific plume, the relative age spectrum can be isolated and integrated over the twenty days and thus, a mean plume age is derived, called hereafter FLEXPART age.

ACPD
12, 4541–4588, 2012

3 Case 1: anthropogenic plume sampled during three consecutive days

During flights on 9, 10 and 11 of April (flight number 33, 34 and 35, respectively), an anthropogenic air mass was sampled during three consecutive days by the ATR-42 French aircraft (see Fig. 1). It originated from areas in Central Europe as seen on the FPES maps shown in Fig. 2 and was sampled at an altitude between 4 and 5 km. The anthropogenic origin of the plume is supported by the fact that no hot spot influence was detected by MODIS. In addition, lagrangian calculations using through the FLEXTRA model show the strong plume coherence between the sampling periods (K. S. Law and J. F. Burkhart, personnal communication, 2011).

3.1 Aerosol size distributions evolution

Figure 3 shows the evolution of the aerosol size distribution along the flight on 9 April. The two measurement periods corresponding to the anthropogenic plume are indicated with red rectangles. A strong Aitken mode appears during the periods when the anthropogenic plume was encountered. For all three flights sampling this air mass, aerosol size distributions averaged over the sampling periods are plotted in Fig. 4. In addition, a typical polar background size distribution is shown in blue. Parametrisations of size distributions calculated from lognormal fits with three size modes, are added in this figure. The log-normal parameters, i.e. the number concentrations N_i, the standard deviation σ_i and the mean diameter D_{mi} related to mode i (ranging from 1 to 3) are reported in Table 1. The highly concentrated Aitken mode (860 cm^{-3}), centered around 33 nm mean diameter for the first sampling flight evolves to larger mean diameters (51 nm for the third flight). This evolution is explained by potential aerosol coagulation and possibly particle growth due to condensation of the gas phase onto pre-existing Aitken mode particles as discussed in Tunved et al. (2004). Notice that the time since emission of the sampled pollution plume increased by about three days between the first and the third flight (Table 1, Fig. 2). The evolution of the aerosol size distribution observed during the three subsequent flights, was simulated using a coagulation model. The results are presented more in detail in Sect. 3.4. Furthermore, the evolution of the

ACPD
12, 4541–4588, 2012

Aitken mode mean diameter as a function of mean air mass age derived from FLEXPART source contributions as a function of time is parameterised with an exponential fit and shown in Fig. 5. According to this parameterisation, Aitken mode particles at the source would have been characterised by a 14.4 nm mean diameter. This result is in agreement with previous studies on urban aerosol nucleation modes (Whitby, 1978; Wehner and Wiedensohler, 2003; Zhang et al., 2004; Hussein et al., 2005; Costabile et al., 2009).

Between the 9 and 11 April, the accumulation mode mean diameter is shifted from 104 to 133 nm and the mean maximum accumulation mode concentration decreased from 920 to 515 cm^{-3} in dN/dlog$D$. The decrease of accumulation mode number concentration (Fig. 5) with ageing is also attributed to coagulation and probably, to a lesser extent, to dilution and dry scavenging processes since no cloud formation occurred during the transport, thus precipitation scavenging can be excluded.

3.2 Refractory aerosol particles

Ambient and elevated (280 °C) temperature systems can give evidence on the state of mixture of aerosol particles, for example, to what extent accumulation mode aerosol particles have been coated. The ambient and heated aerosol number size distributions are presented in Fig. 6a and b for flights on 9, 10 and 11 July. Between the first and third sampling day of the European anthropogenic air mass, ambient (104 to 133 nm) and heated (43.4 to 58.9 nm) accumulation mode modal diameter increased by 29 % whereas the corresponding refractory mode modal diameter (resulting from desorbed ambient accumulation mode) increased by 33 %. $F_{conc,ac}$ is rather constant during the 6 selected periods with a mean value of 1.14, indicating that the entire ambient accumulation mode can be found in the refractory mode (hence shifted to smaller sizes between 43 and 59 nm). This ratio is greater than one since refractory Aitken mode particles may partly appear in the mode of refractory accumulation mode particles. This result highlights the internal mixing of the aerosol accumulation mode of this anthropogenic air mass. $F_{volatile,ac}$ is also rather constant during the two first flights and

ACPD
12, 4541–4588, 2012

decreased during the last flight. Its mean value is 0.79, thus indicating that 79 % of the accumulation mode volume was composed of volatile compounds. Unfortunately, the instrumentation mounted on the ATR-42 did not allow determining the chemical composition of the refractory and volatile aerosol fractions. In addition, the evolution of the Aitken mode after desorption dropped below 20 nm and could not be measured with the NVSMPS system.

3.3 Air mass properties evolution

The evolution of physico-chemical properties of the air masses measured on the ATR-42 and related to the anthropogenic air mass from Central Europe is presented in Figs. 7, 7 and 7. These box plots present the median values as well as 25th and 75th percentiles (box edges) and also the 5th and 95th percentiles (dotted line edges). The mean values are indicated with black dots.

Firstly, Fig. 7 presents the evolution of the enhanced gas phase CO (ΔCO) mixing ratio in ppbv over the background value of 120 ppbv as a function of the FLEXPART age. ΔCO decreases exponentially (fitted black line) with a time scale of $\tau = 6.4$ days. An estimation of the ΔCO concentration near the source region is around 248 ppbv. The rather low correlation coefficient ($r^2 = 0.41$) suggests that the aircraft sampled different parts of the pollution plume with different pollutant loadings. The overall decrease with time is likely due to dilution of the plume.

The light absorption coefficient (σ_{abs}) measured by the PSAP is shown in Fig. 7. The evolution of σ_{abs} as a function of time is exponentially fitted (black line). σ_{abs} decreases exponentially over a period τ of 2.4 days. The difference in period τ of exponential decreasing concentration should be mainly due to the process of gravitational settling of particles, which is not affecting CO. The exponential fit can be used to estimate a light absorption coefficient over the source region of 3.5 Mm^{-1} corresponding to about 300 $ng\,m^{-3}$ of absorbing material. This result is in agreement with recent measurements in the vicinity of European urban areas presented by McMeeking et al. (2010). The measurements are performed at high latitude where Arctic snow cover might be

ACPD
12, 4541–4588, 2012

impacted by dry/wet deposition of black carbon, in addition to the aerosol direct effect of soot particles (Quinn et al., 2008).

Finally, Fig. 7 shows $F_{volatile}$ of the aerosol population as function of the FLEXPART age. This parameter is related to the condensed (rather volatile) material, i.e. coating of aerosol particles. $F_{volatile}$ is constant during the first four periods with a mean value of 0.81 ± 0.09, but decreases over the last two periods. This implies that the relative chemical composition of the particles within the air mass did not change considerably between the first and the second flight.

3.4 Modelling of the coagulation process

The coagulation process appears to have been an efficient process governing the ageing of the European anthropogenic air mass. To confirm this statement, a modelling study of the coagulation process was performed with a time step of 100 s, starting from the mean aerosol size distribution on 9 April and using a semi implicit coagulation model, based on particulate matter volume conservation, as presented in Jacobson (2005). Figure 8 shows the modeled distributions after coagulation superimposed on the measured distributions. The Aitken and accumulation mode parameters related to the observed and simulated distributions are presented in Table 2. Comparing the measurements on 9 to 11 April, the observed Aitken mode modal mean diameter shifted from 32.6 to 50.1 nm, while the simulated modal mean diameter shifted from 32.6 to 41.1 nm. Thus, the simulation can explain about half of the modal mean diameter evolution. Condensation processes are probably responsible for the other half of the growth. Since, coagulation is the only process which impacts particle concentrations, evolution of the simulated Aitken mode modal concentrations are in good agreement, $237\,cm^{-3}$ (on the second day) and $167\,cm^{-3}$ on the third day) are close to the measured concentrations of 313 and $174\,cm^{-3}$ for 10 and 11 April, respectively.

However, the modelling of the accumulation mode particle evolution due to coagulation is less correlated with the observations. Whereas the simulated modal mean diameter shifted from 116.8 to 118.1 nm, the observed modal mean diameter shifted

ACPD
12, 4541–4588, 2012

from 116.8 to 134 nm. Thus, the coagulation explains only 10 % of the modal mean diameter evolution. As demonstrated for the Aitken mode, the accumulation mode modal concentration is matches well the observed (285 cm^{-3}) and simulated (263 cm^{-3}) concentrations on 11 April.

Hence, both the Aitken as well as the accumulation mode modal diameter evolution cannot be explained solely by coagulation. Thus, the processes of condensation and ageing of particulate matter helps to explain the entire modal diameter evolutions. To support the hypothesis, Merlaud et al. (2011) found enhanced gaseous NO_2 concentration measurements in the plume sampled on 9 April. NO_2, through oxidation reactions in the atmosphere, can form N_2O_5 and NO_3 compounds which are able to interact with aerosol particles (Mentel et al., 1996; Hallquist et al., 2000; Benton et al., 2010). However, it is difficult to evaluate the impact of condensation processes since they cannot be simulated without a complete suite of measurements of potential condensable gases. In addition, condensation is, of course, occurring from 9 (and probably before) to 11 April and should impact the modal mean diameter evolutions during all three days of the study. The following relationship links particle diameter to the shift of the diameter due to condensation processes:

$$\frac{dD_p}{dt} = \frac{4D_i M_i}{RTD_p\rho_p} f(Kn,\alpha)(p_i - p_{eq}) \quad (4)$$

with D_i and M_i are diffusion coefficient and molecular weight of the gas i, R is the ideal gas constant, T the medium temperature, ρ_p the particle density, $f(Kn,\alpha)$ is a correction factor related to discontinuity effects and finally, p_i is the partial pressure of the corresponding species while p_{eq} is the total gas pressure at the equilibrium. According to Eq. (4), Aitken mode should have been more impacted by condensation processes than accumulation mode. This would mean that the above described coagulation process should have been more involved in the modal diameter growth than what has been found from the model.

ACPD
12, 4541–4588, 2012

4 Case 2: Eurasian polluted plumes

During flights on 08:00 (a.m. and p.m.), 9, 10 and 11 April, several pollution plumes were sampled by the ATR-42, such as from biomass fires in eastern Europe (north of the Black Sea) and forest fires in Siberia (see Fig. 9). Moreover, air masses with eastern Asia anthropogenic pollution particles were sampled. The Asian plume anthropogenic and biomass burning origins, discussed in Adam de Villiers et al. (2010) are investigated in the subsequent section. Compared to the European anthropogenic plume discussed in the previous section, plumes presented in the following section are referred to as Eurasian pollution plumes.

4.1 Aerosol size distributions

During the POLARCAT-France spring campaign, 6 periods related to Eurasian pollution transported to the Arctic were identified through FLEXPART PES: (i) four plumes corresponding to Russian fires, located at the north of the Black Sea (called hereafter Russian fires) and transported over Europe to the sampling location and (ii) and (iii) two plumes corresponding to air masses containing a mixture of Siberian fires and eastern Asia anthropogenic emissions, called hereafter Asian fires and Asian anthropogenic, respectively. Asian plumes denoted (ii) and (iii) were both transported over the pole to the sampling location and were clearly visible in aerosol Lidar measurements, as presented in Adam de Villiers et al. (2010). Examples of PES corresponding to Russian and Siberian fire origins are presented in Fig. 9. Mean aerosol size distributions and log-normally fitted distributions for the pollution plumes originated from Russian fires, Asian fires, and Asian anthropogenic emissions are shown in Fig. 10. Size distributions related to Russian and Asian fire plumes are plotted in red and green, respectively, while that related to the anthropogenic air masses is plotted in yellow. In order to illustrate the enhancement in particle concentrations over usual Arctic background concentrations, a background aerosol size distribution (selection supported from PES and FPES analysis, indicating local origins) is added in blue on Fig. 10. Parameters

ACPD
12, 4541–4588, 2012

related to the log-normal parameterisations (three or four modes) of the aerosol size distributions are presented in Table 3.

Concerning the observed Eurasian pollution plume, aerosol size distributions are characterized by the highly concentrated accumulation mode and very low Aitken mode particle concentrations as seen in Fig. 10. The FLEXPART ages are reported in Table 3. While the Aitken mode was the main contributor to the total particle concentration of the European anthropogenic plume (Sect. 3), Russian fires and Asian polluted plumes were mostly characterised by large accumulation mode particles. According to these findings, Eurasian pollution plume air masses, especially from anthropogenic origins were expected to be older than the anthropogenic European ones. The air mass ages calculated from FLEXPART for the Eurasian plumes are similar to ages of the European anthropogenic plumes discussed in the previous section.

With respect to the log-normal parameterisations (see Table 3), for Asian air masses, two modes have been necessary in the diameter range usually associated to the accumulation mode (100–300 nm). The first mode with a modal mean diameter of 150 nm is related to forest fires while the second mode, centered on 250 nm, might be linked to anthropogenic emissions. These assumptions are based on Adam de Villiers et al. (2010) who concluded on the intensity of the anthropogenic contribution to these two specific air masses (ii) and (iii). This intensity of the anthropogenic contribution can be seen in the fitted concentrations of the second accumulation mode (149 and 35 cm^{-3}), as shown in Fig. 11b and c. When comparing these air masses to the European air masses, air mass ages (roughly five days) are rather similar. However, aerosol size distributions are completely different for European (first case study) and Asian (second case study) air mass origins. Whereas the European Aitken and accumulation mode maxima are of the order of 2400 and 920 cm^{-3} in dN/dlog$D$ plots, with corresponding mode diameters of 33.1 nm and 116.8 nm, respectively, the maxima are on the order of 240 and 860 cm^{-3} in dN/dlog$D$, with mode diameters of 74.5 nm and 200.1 nm for the Asian plumes (Asian accumulation mode concentrations correspond to the sum of both modelled modes). The differences in the Aitken mode concentration may be explained

ACPD
12, 4541–4588, 2012

by several hypotheses:

- The condensation process may be more significant in Asian air masses because of higher concentrations of condensable material.
- The emission strengths of Aitken mode particles are stronger in Asian air masses, leading to more efficient coagulation of Aitken mode particles.
- Particles emitted from Asian sources are larger, with small amounts of Aitken mode particles.
- Large-scale nucleation events occur in European air masses during transport.

While it is difficult to proof the second, third and fourth hypotheses, the first one will be studied in the following section, presenting the analysis of volatile volume fractions of the aerosol particles.

4.2 Refractory aerosol particles

The volatility behaviour (particle number and volume) of aerosol particles from Russian and Asian fires as well as from Asian anthropogenic sources is derived from ambient and heated number size distributions. Figure 11a presents the mean ambient and desorbed size distribution for Russian fires. As described in the previous section, ambient size distributions are dominated by the highly concentrated accumulation mode. The mean refractory (or desorbed) size distribution shows a similar shape with a highly desorbed former accumulation mode preserving particle concentrations, as seen in the calculated $F_{\mathrm{conc,ac}}$ mean value of 0.96 for the related periods. The mean value of 0.79 for the derived accumulation mode volatile volume fraction $F_{\mathrm{volatile,ac}}$ highlights the high volatility of the accumulation mode of the Russian fire plume particles. This is also illustrated by the important shift in the modal mean diameter from 127.0 to 74.2 nm. A second, but rather refractory mode is found with a very low concentration at a modal diameter of 27 nm.

ACPD
12, 4541–4588, 2012

The Asian air masses (fires and mixed emissions) were also characterised by a highly concentrated accumulation mode (Fig. 11b and c). As mentioned in Sect. 4.1, the accumulation mode is composed of two contributions described by two separate modes (anthropogenic and forest fires, Adam de Villiers et al., 2010) corresponding to mean diameters of roughly 150 and 240 nm, respectively. The mean aerosol distribution associated to Asian fires consisted mainly of a mode with a modal diameter of 154 nm which, after heating, desorbed to an almost mono-modal distribution with a very low concentrated secondary refractive mode (58 cm^{-3}) centered at 27 nm and a highly concentrated mode (393 cm^{-3}) centered at 78 nm. This means that the evolution of aerosol distributions from Asian fires and Russian fires is very similar.

The anthropogenically influenced aerosol distribution at ambient temperature was mostly composed of a first mode with mean diameter of 141 nm and a concentration of 433 cm^{-3} and a second mode centered at 253 nm with a concentration of 171 cm^{-3}. After desorption, the refractory aerosol size distribution presents three refractory modes. Two of them were centered at 27 and 75 nm with a cumulated concentration of 440 cm^{-3} while the third mode was centered at 150 nm with a modal concentration of 160 cm^{-3}. Regarding the modal diameters and concentrations of the three modes and what we learned from size distributions clearly related to fires, the first two modes then are associated to Asian fire emissions while the third mode is attributed to a contribution from Asian anthropogenic emissions. A similar behaviour of an anthropogenic air mass was already presented by Pratt and Prather (2009) who observed aged urban particles, mostly composed of organic material, at ambient temperature and 230 °C and found modal mean diameters of 242 and 177 nm, respectively.

5 In-situ samples

During the five last flights of the campaign, seven aerosol in-situ samples were collected in clear sky conditions. Table 4 summarizes information about the samples including the origin of the sampled air masses, flight dates, start and end time of

ACPD
12, 4541–4588, 2012

sampling, and the corresponding relative humidity (RH). Figure 12 presents typical images of submicron aerosol particles sampled in different air masses. Clean polar air mass images clearly show satellite-like particles with a large drop surrounded by smaller droplets, as seen in Fig. 12a, which are typically a signature of acidic sulphate. The supposed acidity and absence of soot both indicates that the particles were not in close contact with the continental air masses. No obvious differences can be found between Russian fire and European anthropogenic particles, as shown in Fig. 12b and c where many particles left liquid like stain and soot like inclusions. RH may have had influence on the formation of the coating layer because those in Fig. 12d seem to have more solid, crystalline like structure. Fig. 12d images are for RH of 23 % while Fig. 12b and c images are for RH > 40 %. Otherwise, the elements comprising the forest fire and anthropogenic particles were rather common.

The detection frequencies (DF) and atomic ratio (AR) of several elements found in analysed submicron aerosol samples are presented in Fig. 13. Sulphur (S) is a major compound of sulphuric acid and sulphate and it is not surprising to find it with a 100 % DF. However, sulphur is more concentrated in anthropogenic particles with an AR about 80 %. Potassium (K) is considered as a biomass burning tracer (Andreae, 1983) but can be measured, to a lower extent, in fossil fuel emissions, too (Guazzotti et al., 2003). As shown in Fig. 13, almost all particles from fire origins contain K while the DF of K decreases to 60 % for anthropogenic particles and 20 % for clean polar air. This trend in DF is similar in the AR (Fig. 13). DF of soot-like inclusions depends on air mass origins but cannot be clearly related to fire or anthropogenic origins. Analyses of supermicron samples mainly pointed out the predominence of alumino-silicate mineral dust particles, and to a lesser extent by sea salt. Unlike submicron particles, no clear-cut correlation regarding the air mass origins were found.

ACPD
12, 4541–4588, 2012

6 Conclusions

This study focuses on the characterisation of pollution plumes transported to the Scandinavian Arctic during spring of the year 2008. Two studies of transported air masses are presented here. Therein, the first case study investigates an European anthropogenic plume sampled during three consecutive flights. On the one hand, aerosol size distributions related to this plume illustrate particularly well the ageing of observed Aitken mode where concentration is decreasing (from 860 to 165 cm^{-3} in dN/dlog$D$) and mean Aitken mode diameter is increasing (from 33 to 51 nm) with plume age increasing from 5.0 ± 0.2 to 7.7 ± 0.1 days. Half of the Aitken mode evolution could be reproduced using a semi-implicit coagulation model, suggesting that the coagulation process was at least as important as condensation processes in the evolution of the Aitken mode particle diameters. In addition, the simulated Aitken mode modal concentrations were similar to the observations. Whereas the simulated accumulation mode concentration was in agreement with the observations, the accumulation mode modal mean diameter evolution was less well reproduced by the coagulation model: only 10 % of the modal diameter evolution can be related to the coagulation process. Thus, gas phase condensation is also likely to have contributes, even if the volatile fraction, mostly related to condensable materials on particles, was the same for the three days.

Related parameters like mean diameter of the Aitken mode, ΔCO mixing ratio, and the light absorption coefficient σ_{abs} exponentially decreased with ageing of the plume. According to these exponential parameterisations, extrapolations of trends woulf infer that Aitken mode particles were emitted with an estimated mean diameter of 14.4 nm, coupled to an estimated light absorption coefficient of 3.5 Mm^{-1} (equivalent to 300 ng m^{-3} of absorbing material, i.e. black carbon) and an estimated ΔCO mixing ratio of 248 ppbv. These values are in agreement with measurements performed over urban areas. This finding is also supported by the refractory distributions demonstrating that the Aitken mode particles were desorbed to sizes below the instrument lower detection limit of 20 nm. The modal mean diameter of the refractory mode desorbed

ACPD
12, 4541–4588, 2012

from the accumulation mode is increasing with time. This evolution is probably due to the ageing of organic materials. This growth in refractory core may compensate the gas phase condensation on particles and explain why the volatile volume fraction is constant.

The second case study focuses on air masses originating from Russia (north of Black Sea) and Asia (trnasported across the North Pole). Russian air masses were mostly influenced by large forest fires and present almost mono-modal aerosol number size distributions, on average, centered around 127 nm in the accumulation mode size range. This mode desorbed into a mode centered at 74 nm which means that aerosols in the russian fire plumes were internally mixed. Aerosols in Asian air masses had a more complex behaviour since their accumulation modes were found externally mixed and composed of two contributions (Adam de Villiers et al., 2010) from biomass burning and anthropogenic emissions with modal mean diameter at 150 and 240 nm, respectively. These two contributions desorbed in two separate modes centered at 75 and 150 nm, thus corresponding to biomass burning and anthropogenic contributions, respectively. The modal concentrations were consistent in both ambient and refractory modes.

Finally, in-situ submicron and supermicron aerosol particles samples were collected during the flights. Clear differences were found for plumes with different origins especially with respect to the potassium detection frequency and atomic ratio, which is highest in fire samples, then decreases for anthropogenic samples, and is lowest for clean air polar air masses. In addition, particle images confirm differences between clean and polluted air mass origins of aerosol particles.

Acknowledgements. The authors would like to thank the French research agencies ANR, CNES, CNRS-INSU, and IPEV as well as EUFAR and CLIMSLIP-LEFE. NILU researchers were supported by the Norwegian Research Council in the framework of POLARCAT-Norway and CLIMSLIP. We also would like to thank SAFIRE and Christophe Gourbeyre for their support during the planning and execution of the French ATR-42 campaigns and, together with DT-INSU, for help with instrument integration.

ACPD
12, 4541–4588, 2012

The publication of this article is financed by CNRS-INSU.

References

Albrecht, B. A.: Aerosols, Cloud Microphysics, and Fractional Cloudiness, Science, 245, 1227–1230, 1989. 4543

Andreae, M. O.: Soot carbon and excess fine potassium: Long-range transport of combustion-derived aerosols, Science, 220, 1148–1151, 1983. 4559

Benton, A. K., Langridge, J. M., Ball, S. M., Bloss, W. J., Dall'Osto, M., Nemitz, E., Harrison, R. M., and Jones, R. L.: Night-time chemistry above London: measurements of NO_3 and N_2O_5 from the BT Tower, Atmos. Chem. Phys., 10, 9781–9795, doi:10.5194/acp-10-9781-2010, 2010. 4554

Bond, T. C., Anderson, T. L., and Campbell, D.: Calibration and intercomparison of filter-based measurements of visible light absorption by aerosols, Aerosol Sci. Technol., 30, 582–600, 1999. 4547

Brock, C., Radke, L., and Hobbs, P.: Sulfur in particles in Arctic hazes derived from airborne in situ and lidar measurements, J. Geophys. Res., 95, 22369–22387, 1990. 4543

Brock, C. A., Cozic, J., Bahreini, R., Froyd, K. D., Middlebrook, A. M., McComiskey, A., Brioude, J., Cooper, O. R., Stohl, A., Aikin, K. C., de Gouw, J. A., Fahey, D. W., Ferrare, R. A., Gao, R.-S., Gore, W., Holloway, J. S., Hübler, G., Jefferson, A., Lack, D. A., Lance, S., Moore, R. H., Murphy, D. M., Nenes, A., Novelli, P. C., Nowak, J. B., Ogren, J. A., Peischl, J., Pierce, R. B., Pilewskie, P., Quinn, P. K., Ryerson, T. B., Schmidt, K. S., Schwarz, J. P., Sodemann, H., Spackman, J. R., Stark, H., Thomson, D. S., Thornberry, T., Veres, P., Watts, L. A., Warneke, C., and Wollny, A. G.: Characteristics, sources, and transport of aerosols measured in spring 2008 during the aerosol, radiation, and cloud processes affecting Arctic Climate (ARCPAC) Project, Atmos. Chem. Phys., 11, 2423–2453, doi:10.5194/acp-11-2423-2011, 2011. 4543

Clarke, A. D., Charlson, R. J., and Radke, L. F.: Airborne observations of Arctic aerosols. IV: Optical properties of Arctic Haze, Geophys. Res. Lett., 11, 405–408, doi:10.1029/GL011i005p00405, 1984. 4543

Costabile, F., Birmili, W., Klose, S., Tuch, T., Wehner, B., Wiedensohler, A., Franck, U., König, K., and Sonntag, A.: Spatio-temporal variability and principal components of the particle number size distribution in an urban atmosphere, Atmos. Chem. Phys., 9, 3163–3195, doi:10.5194/acp-9-3163-2009, 2009. 4551

Adam de Villiers, R., Ancellet, G., Pelon, J., Quennehen, B., Schwarzenboeck, A., Gayet, J. F., and Law, K. S.: Airborne measurements of aerosol optical properties related to early spring transport of mid-latitude sources into the Arctic, Atmos. Chem. Phys., 10, 5011–5030, doi:10.5194/acp-10-5011-2010, 2010. 4545, 4548, 4555, 4556, 4558, 4561

Dreiling, V. and Friederich, B.: Spatial distribution of the arctic haze aerosol size distribution in western and eastern Arctic, Atmos. Res., 44, 133–152, doi:10.1016/S0169-8095(96)00035-X, 1997. 4543

Forster, C., Wandinger, U., Wotawa, G., James, P., Mattis, I., Althausen, D., Simmonds, P., O'Doherty, S., Jennings, S. G., Kleefeld, C., Schneider, J., Trickl, T., Kreipl, S., Jäger, H., and Stohl, A.: Transport of boreal forest fire emissions from Canada to Europe, J. Geophys. Res., 106, 22887–22906, doi:10.1029/2001JD900115, 2001. 4548

Frossard, A. A., Shaw, P., Russell, L. M., Kroll, J. H., Canagaratna, M. J., Worsnop, D. R., Quinn, P. K., and Bates, T. S.: Springtime Arctic haze contributions of submicron organic particles from European and Asian combustion sources, J. Geophys. Res., 116, D05205, doi:10.1029/2010JD015178, 2011. 4543

Garrett, T. J. and Zhao, C.: Increased Arctic cloud longwave emissivity associated with pollution from mid-latitudes, Nature, 440, 787–789, 2006. 4543

Giglio, L., Descloitres, J., Justice, C. O., and Kaufman, Y.: An enhanced contextual fire detection algorithm for MODIS, Remote Sens. Environ., 87, 273–282, doi:10.1016/S0034-4257(03)00184-6, 2003. 4549

Greenaway, K. R.: Experiences with Arctic flying weather, Royal Meteorol. Soc. Can. Branch, Toronto, Ont., Canada, 1950. 4543

Guazzotti, S. A., Suess, D. T., Coffee, K. R., Quinn, P. K., Bates, T. S., Wisthaler, A., Hansel, A., Ball, W. P., Dickerson, R. R., Neususs, C., Crutzen, P. J., and Prather, K. A.: Characterization of carbonaceous aerosols outflow from India and Arabia: Biomass/biofuel burning and fossil fuel combustion, J. Geophys. Res., 108, 4485, doi:10.1029/2002JD003277, 2003. 4559

ACPD
12, 4541–4588, 2012

Hallquist, M., Stewart, D. J., Baker, J., and Cox, R. A.: Hydrolysis of N_2O_5 on submicron sulfuric acid aerosols, J. Phys. Chem. A, 104, 3984–3990, 2000. 4554

Hinds, W. C.: Aerosol technology: properties, behaviour and measurement of airborne particles, Wiley-Interscience, 1999. 4544

Hirdman, D., Sodemann, H., Eckhardt, S., Burkhart, J. F., Jefferson, A., Mefford, T., Quinn, P. K., Sharma, S., Ström, J., and Stohl, A.: Source identification of short-lived air pollutants in the Arctic using statistical analysis of measurement data and particle dispersion model output, Atmos. Chem. Phys., 10, 669–693, doi:10.5194/acp-10-669-2010, 2010. 4543

Huang, L., Gong, S. L., Sharma, S., Lavoué, D., and Jia, C. Q.: A trajectory analysis of atmospheric transport of black carbon aerosols to Canadian high Arctic in winter and spring (1990–2005), Atmos. Chem. Phys., 10, 5065–5073, doi:10.5194/acp-10-5065-2010, 2010. 4543

Hussein, T., Hämeri, K., Aalto, P., Paatero, P., and Kulmala, M.: Modal structure and spatial-temporal variations of urban and suburban aerosols in Helsinki, FInland, Atmos. Environ., 39, 1655–1668, doi:10.1016/j.atmosenv.2004.11.031, 2005. 4551

IPCC: Climate Change 2007: Synthesis Report. Contribution of Working groups I, II and III to the fourth Assessement Report of the Intergouvernemental Panel on Climate Change, edited by: Core Writing Team, Pachauri, R. K., and Reisinger, A., IPCC, Geneva, Switzerland, 2007. 4543

Jacobson, M. Z.: Fundamentals of atmospheric modeling, second edition, Cambridge University press, Cambridge, UK, 2005. 4553

Law, K. S. and Stohl, A.: Arctic Air Pollution: Origins and Impacts, Science, 315, 1537–1540, doi:10.1126/science.1137695, 2007. 4543

Lubin, D. and Vogelmann, A. M.: A climatologically significant aerosol longwave indirect effect in the Arctic, Nature, 439, 453–456, 2006. 4543

Matsuki, A., Iwasaka, Y., Shi, G. Y., Chen, H. B., Osada, K., Zhang, D., Kido, M., Inomata, Y., Kim, Y. S., Trochkine, D., Nishita, C., Yamada, M., Nagatani, M., and Nakata, H.: Heterogeneous sulfate formation on dust surface and its dependence on mineralogy: Balloon-borne measurements in the surface atmosphere of Beijing, China, Water, Air and Soil Pollution: Focus, 5, 101–132, 2005a. 4548

Matsuki, A., Iwasaka, Y., Shi, G. Y., Zhang, D., Trochkine, D., Yamada, M., Kim, Y. S., Chen, B., Nagatani, T., Miyazawa, T., Nagatani, M., and Nakata, H.: Morphological and chemical modification of mineral dust: Observational insight into the heterogeneous uptake of acidic

ACPD
12, 4541–4588, 2012

gases, Geophys. Res. Lett., 32, L22806, doi:10.1029/2005GL024176, 2005b. 4548
Matsuki, A., Quennehen, B., Schwarzenboeck, A., Crumeyrolle, S., Venzac, H., Laj, P., and Gomes, L.: Temporal and vertical variations of aerosol physical and chemical properties over West Africa: AMMA aircraft campaign in summer 2006, Atmos. Chem. Phys., 10, 8437–8451, doi:10.5194/acp-10-8437-2010, 2010. 4548
McCormick, R. A. and Ludwig, H.: Climate modification by atmospheric aerosols, Science, 156, 1358–1359, 1967. 4543
McMeeking, G. R., Hamburger, T., Liu, D., Flynn, M., Morgan, W. T., Northway, M., Highwood, E. J., Krejci, R., Allan, J. D., Minikin, A., and Coe, H.: Black carbon measurements in the boundary layer over western and northern Europe, Atmos. Chem. Phys., 10, 9393–9414, doi:10.5194/acp-10-9393-2010, 2010. 4552
Mentel, T. F., Bleilebens, D., and Wahner, A.: A study of nighttime nitrogen oxide oxidation in a large reaction chamber – The fate of NO_2, N_2O_5, HNO_3, and O_3 at different humidities, Atmos. Environ., 30, 4007–4020, 1996. 4554
Merlaud, A., Van Roozendael, M., Theys, N., Fayt, C., Hermans, C., Quennehen, B., Schwarzenboeck, A., Ancellet, G., Pommier, M., Pelon, J., Burkhart, J., Stohl, A., and De Mazière, M.: Airborne DOAS measurements in Arctic: vertical distributions of aerosol extinction coefficient and NO_2 concentration, Atmos. Chem. Phys., 11, 9219–9236, doi:10.5194/acp-11-9219-2011, 2011. 4543, 4545, 4549, 4554
Mitchell, J. M.: Visual range in the polar regions with particular reference to the Alaskan Arctic, J. Atmos. Terr. Phys. Spec., Suppl., 195–211, 1957. 4543
Nédélec, P., Cammas, J.-P., Thouret, V., Athier, G., Cousin, J.-M., Legrand, C., Abonnel, C., Lecoeur, F., Cayez, G., and Marizy, C.: An improved infrared carbon monoxide analyser for routine measurements aboard commercial Airbus aircraft: technical validation and first scientific results of the MOZAIC III programme, Atmos. Chem. Phys., 3, 1551–1564, doi:10.5194/acp-3-1551-2003, 2003. 4548
Pratt, K. A. and Prather, K. A.: Real-time, single-particle volatility, size, and chemical composition measurements of aged urban aerosols, Environ. Sci. Technol., 43, 8276–8282, doi:10.1021/es902002t, 2009. 4558
Quennehen, B., Schwarzenboeck, A., Schmale, J., Schneider, J., Sodemann, H., Stohl, A., Ancellet, G., Crumeyrolle, S., and Law, K. S.: Physical and chemical properties of pollution aerosol particles transported from North America to Greenland as measured during the POLARCAT summer campaign, Atmos. Chem. Phys., 11, 10947–10963, doi:10.5194/acp-

ACPD
12, 4541–4588, 2012

11-10947-2011, 2011. 4545, 4547
Quinn, P. K., Miller, T. L., Bates, T. S., Ogren, J. A., Andrews, E., and Shaw, G. E.: A three-year record of simultaneously measured aerosol chemical and optical properties at Barrow, Alaska, J. Geophys. Res., 107, 4130, doi:10.1029/2001JD001248, 2002. 4543
Quinn, P. K., Shaw, G., Andrews, E., Dutton, E. G., Ruoho-Airola, T., and Gong, S. L.: Arctic Haze: Current trend and knowledge gaps, Tellus B, 59, 99–114, doi:10.1111/j.1600-0889.2006.00238.x, 2007. 4543
Quinn, P. K., Bates, T. S., Baum, E., Doubleday, N., Fiore, A. M., Flanner, M., Fridlind, A., Garrett, T. J., Koch, D., Menon, S., Shindell, D., Stohl, A., and Warren, S. G.: Short-lived pollutants in the Arctic: their climate impact and possible mitigation strategies, Atmos. Chem. Phys., 8, 1723–1735, doi:10.5194/acp-8-1723-2008, 2008. 4553
Schmale, J., Schneider, J., Ancellet, G., Quennehen, B., Stohl, A., Sodemann, H., Burkhart, J. F., Hamburger, T., Arnold, S. R., Schwarzenboeck, A., Borrmann, S., and Law, K. S.: Source identification and airborne chemical characterisation of aerosol pollution from long-range transport over Greenland during POLARCAT summer campaign 2008, Atmos. Chem. Phys., 11, 10097–10123, doi:10.5194/acp-11-10097-2011, 2011. 4545
Schnell, R. C.: Arctic haze and the Arctic Gas and Aerosol Sampling Program (AGASP), Geophys. Res. Lett., 11, 361–364, doi:10.1029/GL011i005p00361, 1984. 4543
Schwarzenboeck, A., Heintzenberg, J., and Mertes, M.: Incorporation of aerosol particles between 25 and 850 nm into cloud element: measurements with a new complementary sampling system, Atmos. Res., 52, 241–260, 2000. 4546
Seinfeld, J. H. and Pandis, S. N.: Atmospheric chemistry & physics, John Wiley & Sons, New York, 1998. 4544
Sharma, S., Brook, J. R., Cachier, H., Chow, J., Gaudenzi, A., and Lu, G.: Light absorption and thermal measurements of black carbon in different regions of Canada, J. Geophys. Res., 107, 4771, doi:10.1029/2002JD002496, 2002. 4543
Sharma, S., Lavoué, D., Cachier, H., Barrie, L. A., and Gong, S. L.: Long-term trends of black carbon concentrations in the Canadian Arctic, J. Geophys. Res., 109, D15203, doi:10.1029/2003JD004331, 2004. 4543
Sharma, S., Andrews, E., Barrie, L. A., Ogren, J. A., and Lavoué, D.: Variations and sources of the equivalent black carbon in the high Arctic revealed by long-term observations at Alert and Barrow 1989–2003, J. Geophys. Res., 111, D14208, doi:10.1029/2005JD006581, 2006. 4543

ACPD
12, 4541–4588, 2012

Springston, S. R. and Sedlacek, A. J. I.: Noise characteristics of an instrumental particle absorbance technique, Aerosol Sci. Technol., 41, 1110–1116, doi:10.1080/02786820701777457, 2007. 4547
Stohl, A.: Characteristics of atmospheric transport into the Arctic troposphere, J. Geophys. Res., 111, 0148–0227, doi:10.1029/2005JD006888, 2006. 4543
Stohl, A., Hittenberger, M., and Wotawa, G.: Validation of the lagrangian particle dispersion model FLEXPART against large-scale tracer experiment data, Atmos. Environ., 32, 4245–4264, doi:10.1016/S1352-2310(98)00184-8, 1998. 4549
Stohl, A., Forster, C., Eckhardt, S., Spichtinger, N., Huntrieser, H., Heland, J., Schlager, H., Wilhelm, F., Arnold, F., and Cooper, O.: backward modeling study of intercontinental pollution transport using aircraft measurements, J. Geophys. Res., 108, 4370, doi:10.1029/2002JD002862, 2003. 4549
Stohl, A., Forster, C., Frank, A., Seibert, P., and Wotawa, G.: Technical note: The Lagrangian particle dispersion model FLEXPART version 6.2, Atmos. Chem. Phys., 5, 2461–2474, doi:10.5194/acp-5-2461-2005, 2005. 4549
Tunved, P., Ström, J., and Hansson, H.-C.: An investigation of processes controlling the evolution of the boundary layer aerosol size distribution properties at the Swedish background station Aspvreten, Atmos. Chem. Phys., 4, 2581–2592, doi:10.5194/acp-4-2581-2004, 2004. 4550
Twomey, S.: The Influence of Pollution on the Shortwave Albedo of Clouds, J. Atmos. Sci., 34, 1149–1152, doi:10.1175/1520-0469(1977)034¡1149:TIOPOT¿2.0.CO;2, 1977. 4543
Villani, P., Picard, D., Michaud, V., Laj, P., and Wiedensohler, A.: Design and Validation of a Volatility Hygroscopic Tandem Differential Mobility Analyzer (VH-TDMA) to Characterize the Relationships Between the Thermal and Hygroscopic Properties of Atmospheric Aerosol Particles, Aerosol Sci. Technol., 42, 729–741, 2008. 4546
Wehner, B. and Wiedensohler, A.: Long term measurements of submicrometer urban aerosols: statistical analysis for correlations with meteorological conditions and trace gases, Atmos. Chem. Phys., 3, 867–879, doi:10.5194/acp-3-867-2003, 2003. 4551
Whitby, K. T.: The physical characteristics of sulphur aerosols, Atmos. Environ., 12, 135–159, 1978. 4551
Zhang, K. M., Wexler, A. S., Zhu, Y. F., Hinds, W. C., and Sioutas, C.: Evolution of particle number distribution near roadways. Part II: the Road-to-Ambient process, Atmos. Environ., 38, 6655–6665, doi:10.1016/j.atmosenv.2004.06.044, 2004. 4551

ACPD
12, 4541–4588, 2012

Table 1. Parameterisation of log-normally fitted size distributions for the anthropogenic plume. FLEXPART determined air mass ages are also indicated.

Flight date	Flexpart age	Aitken mode			Accumulation mode			Coarse mode		
	(days)	n_1(cm^{-3})	σ_1	d_{m1}(nm)	n_2(cm^{-3})	σ_2	d_{m2}(nm)	n_3(cm^{-3})	σ_3	d_{m3}(nm)
9 April	4.7	621	1.35	33.1	621	1.80	108.8	0.018	1.30	2000
	5.3	981	1.36	32.2	556	1.80	124.8	0.001	1.30	2000
10 April	6.7	132	1.29	38.2	595	1.80	118.5	0.046	1.30	2000
	7.1	495	1.44	42.7	402	1.69	139.4	0.024	1.30	2000
11 April	7.6	139	1.36	48.4	407	1.79	116.5	0.102	1.32	1462
	7.8	210	1.54	51.9	163	1.47	151	20.00	2.00	800
Background		84.8	1.80	61.2	157.7	1.62	165.6	0.303	1.30	941

ACPD
12, 4541–4588, 2012

Table 2. Comparison between log-normally fitted observed and simulated aerosol number size distribution parameters.

Flight date		Aitken mode			Accumulation mode		
		n_1(cm^{-3})	σ_1	d_{m1}(nm)	n_2(cm^{-3})	σ_2	d_{m2}(nm)
10 April	Obs.	313	1.36	40.4	493	1.75	128.9
	Sim.	237	1.30	38.8	321	1.70	115.0
11 April	Obs.	174	1.45	50.1	285	1.63	134,0
	Sim.	166	1.30	41.1	263	1.65	118.1

ACPD
12, 4541–4588, 2012

Table 3. Parameterisation of log-normally fitted size distributions for forest fire plumes. FLEXPART determined air mass ages are also indicated.

Air mass type	Flexpart age (days)	Aitken mode			Accumulation mode 1			Accumulation mode 2			Coarse mode		
		n_1(cm^{-3})	σ_1	d_{m1}(nm)	n_2(cm^{-3})	σ_2	d_{m2}(nm)	n_3(cm^{-3})	σ_3	d_{m3}(nm)	n_4(cm^{-3})	σ_4	d_{m4}(nm)
Russian fires	5.3	25.6	1.43	26.5	488	1.62	125.5	–	–	–	2.2	1.57	700
	5.5	8.4	1.4	27.7	515	1.61	131.2	–	–	–	1.81	1.53	700
	6.8	7.9	1.26	26.0	565	1.61	143.5	–	–	–	1.75	1.57	700
	7.4	332	1.60	101.6	182.9	1.50	183.2	–	–	–	1.39	1.45	700
Asian anth.	5	7.8	1.20	32.5	433	1.67	145.4	149	1.37	253.3	0,88	1.30	852
Asian fires	6.6	3.9	1.45	39.9	380	1.67	150.2	36	1.30	249.9	0.34	1.52	1271
Background		84.8	1.80	61.2	157	1.62	165.6	–	–	–	0.303	1.30	941

ACPD
12, 4541–4588, 2012

Table 4. TEM-EDX (submicron) and SEM-EDX (supermicron) samples of individual particles analysed for this study.

Air mass type	date	start time (HH:MM UTC)	end time (HH:MM UTC)	submicronic analysis	RH (%)
European anth.	9 April	09:39	09:47	analysed	38.1
Russian fires	8 April	08:48	09:04	analysed	99
	8 April	13:52	13:59	analysed	82.6
	9 April	12:04	12:17	analysed	55.0
Asian anth.	11 April	10:42	10:52	analysed	22.7
Polar clear air	8 April	09:33	09:37	analysed	26.3
	11 April	12:16	12:27	analysed	55.8

ACPD
12, 4541–4588, 2012

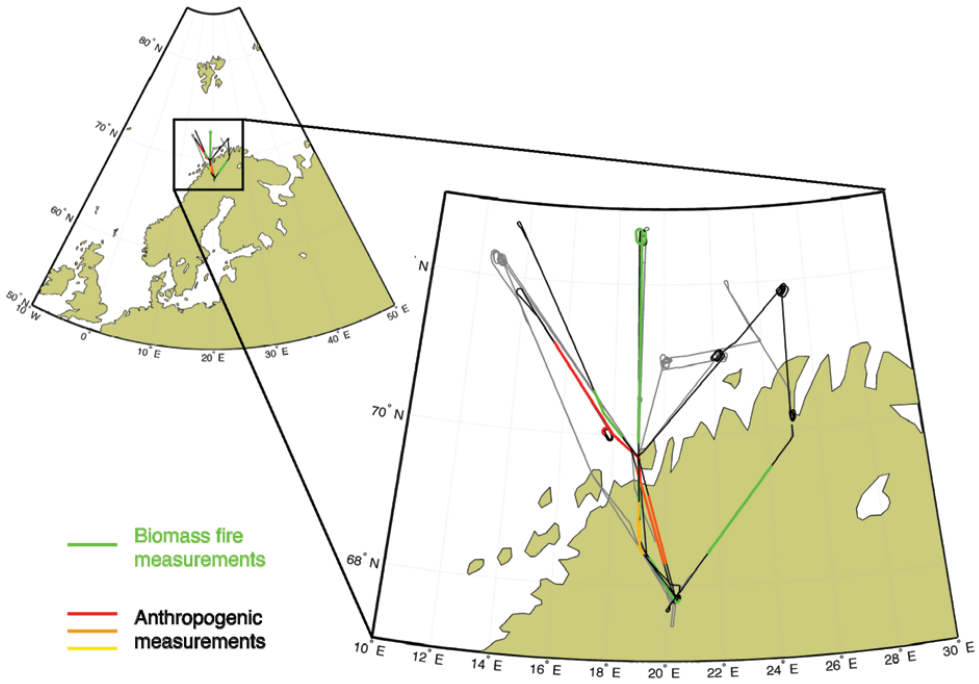

Fig. 1. ATR-42 flight tracks highlighting the legs on which forest fire and anthropogenic plumes were sampled.

ACPD
12, 4541–4588, 2012

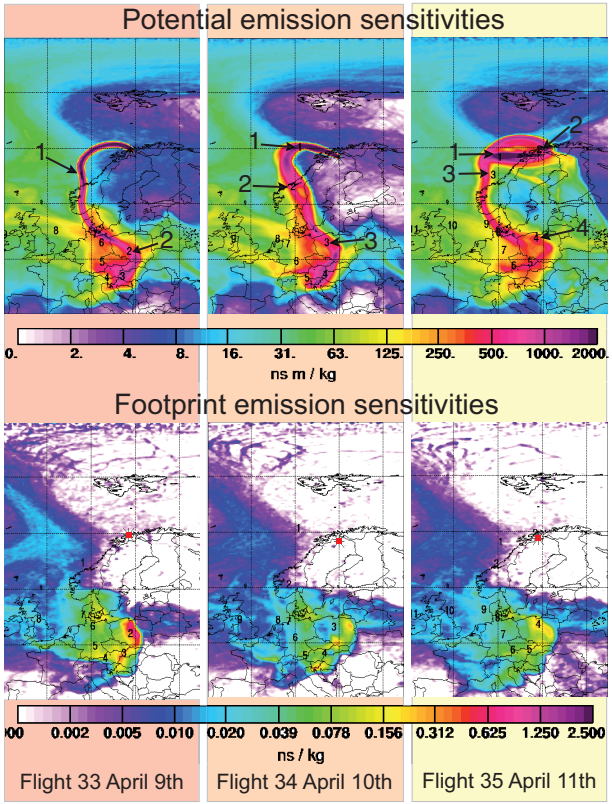

Fig. 2. FLEXPART column-integrated potential emission sensitivities (PES, top) and footprint emission sensitivities (FPES, bottom) for the anthropogenic air mass sampled during the flights on 9, 10 and 11 April 2008. Numbers indicate the air mass age in days at the location pointed by corresponding black arrows. On FES maps, red squares indicate the aircraft location, used as a starting point to run FLEXPART.

ACPD
12, 4541–4588, 2012

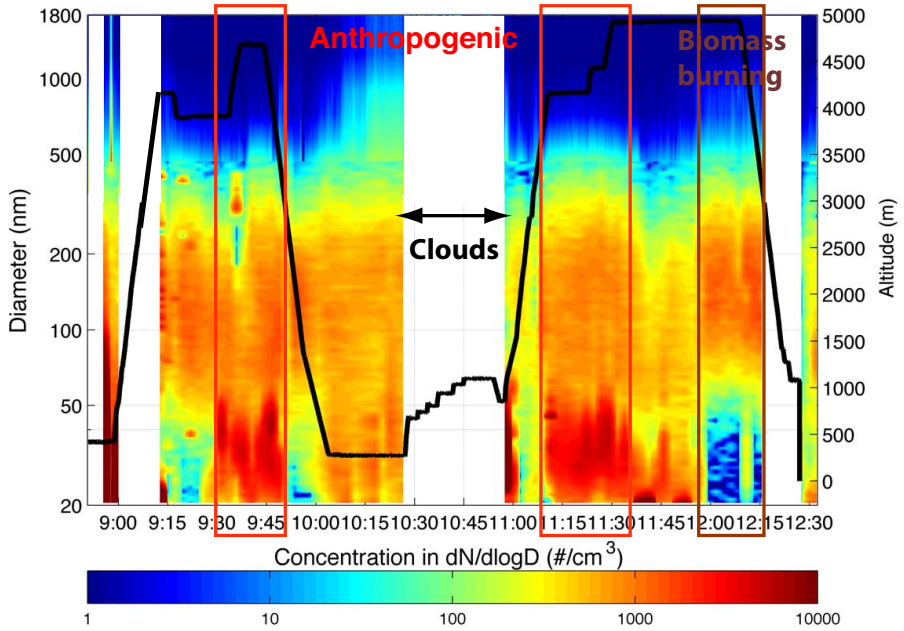

Fig. 3. Evolution of the aerosol size distribution along the flight on 9 April. While the principal y-axis (left) shows the diameter related to the colour coded concentrations, the secondary y-axis (right) corresponds to the flight altitude plotted in black. Sampling periods related to anthropogenic and forest fire plumes are indicated with red and brown rectangles, respectively.

ACPD
12, 4541–4588, 2012

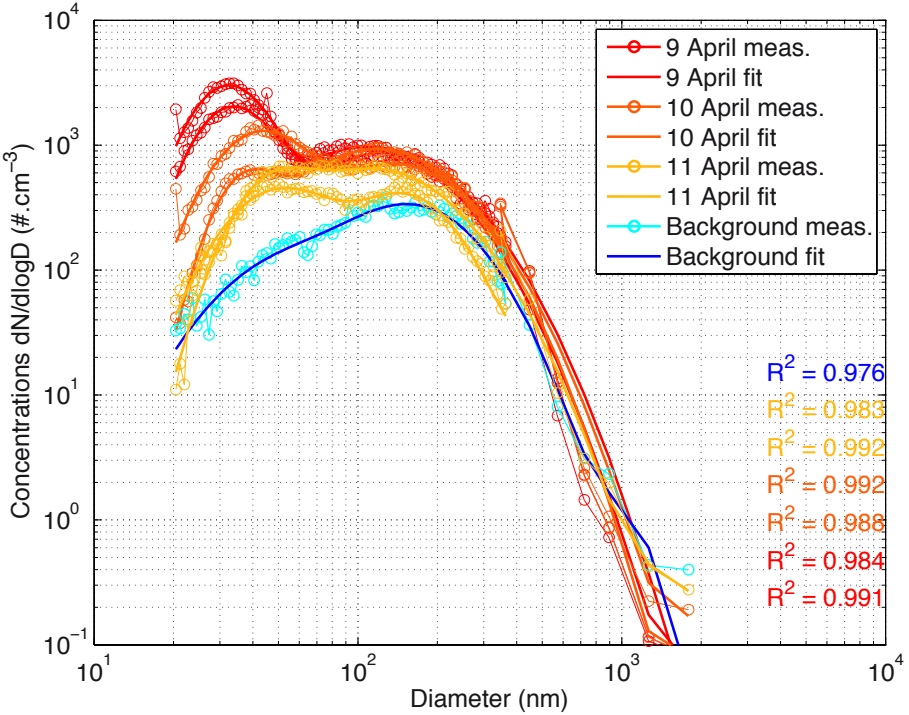

Fig. 4. Anthropogenic aerosol size distributions measured (thin solid line with circles) and fitted (thick solid line) for flights on 9, 10 and 11 April coloured in red, orange and yellow, respectively. A typical background size distribution encountered in non polluted air masses is shown in blue. Distributions are fitted with a 3 log-normal parameterisation, corresponding correlation factors are indicated.

ACPD
12, 4541–4588, 2012

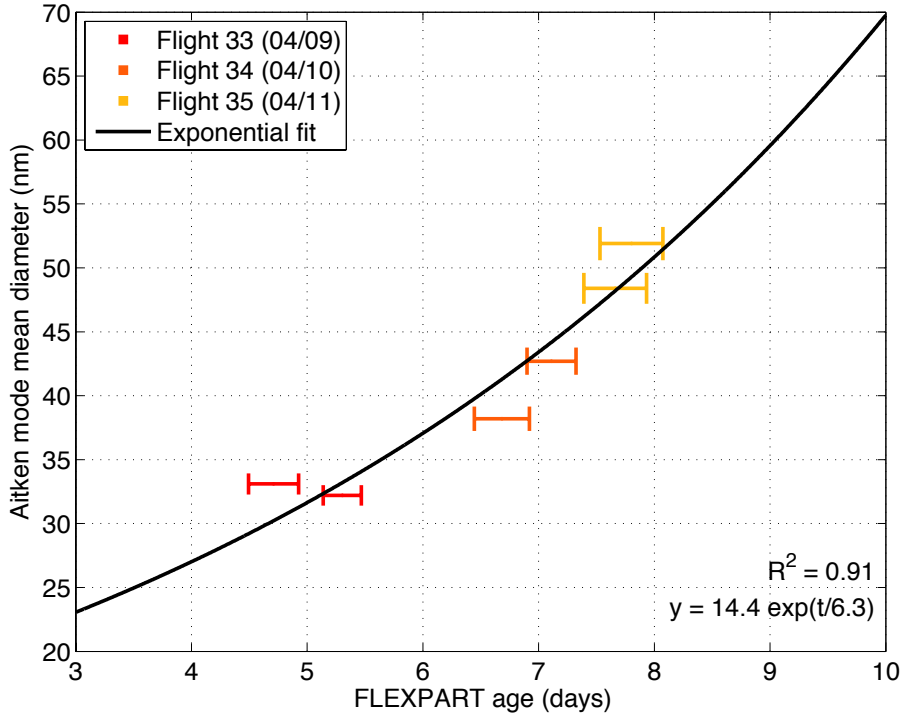

Fig. 5a. Evolution of the Aitken mode mean diameter as a function of the FLEXPART age for the anthropogenic plume. Data points are colour coded with respect to the flight dates. An exponential fit shown as a black line.

ACPD
12, 4541–4588, 2012

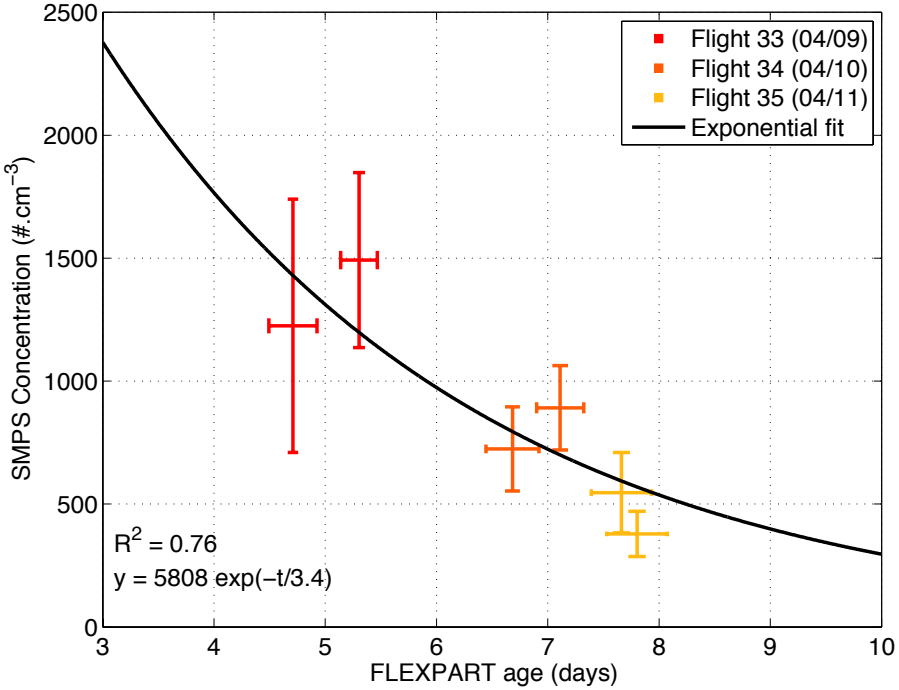

Fig. 5b. Evolution of the SMPS concentration (20–450 nm) as a function of the FLEXPART age for the anthropogenic plume. Data points are colour coded with respect to flight dates and an exponential fit is shown as a black line.

ACPD
12, 4541–4588, 2012

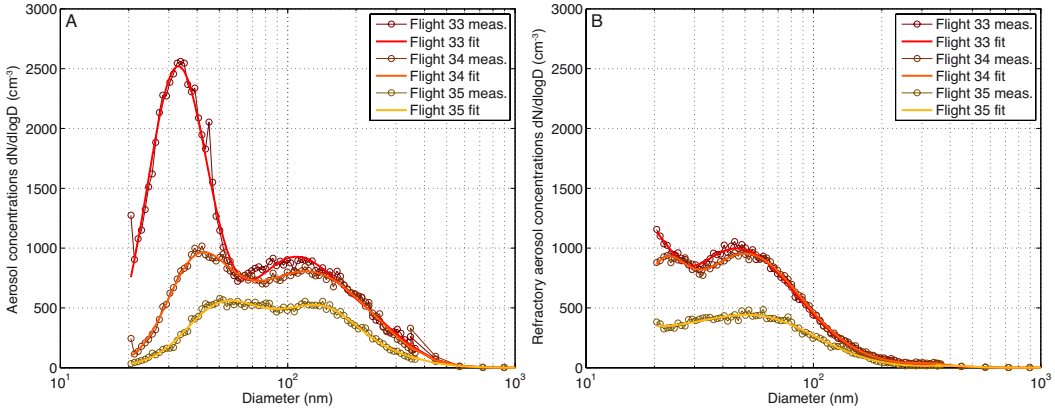

Fig. 6. (A) Ambient and **(B)** 280 °C aerosol number size distributions for flights on 9, 10 and 11 April.

ACPD
12, 4541–4588, 2012

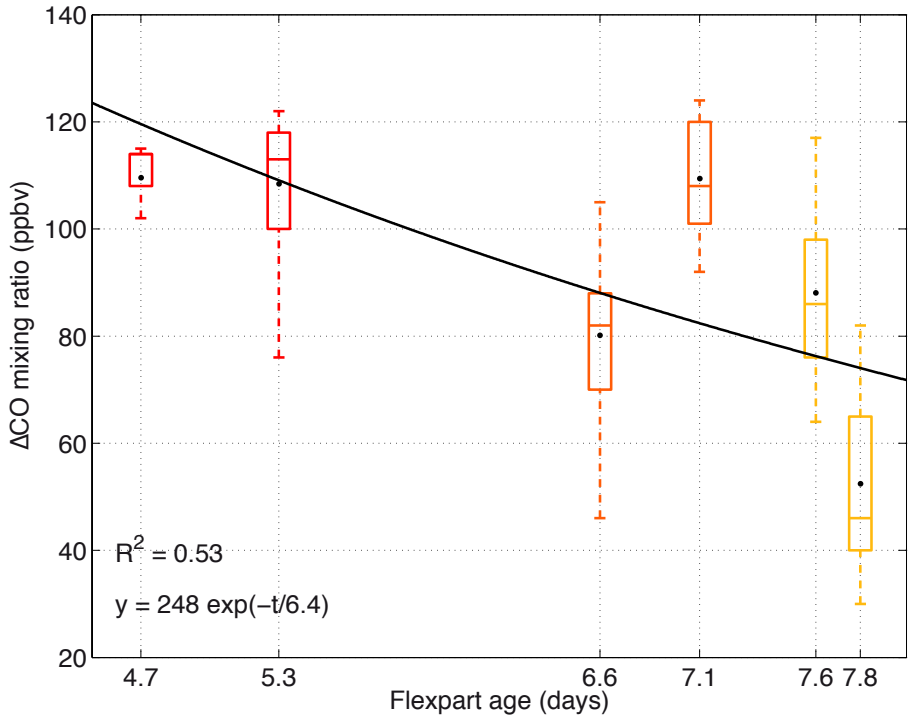

Fig. 7a. Evolution of the enhanced carbon monoxide mixing ratios (ppbv) as a function of FLEXPART age for the anthropogenic plume samplings. An exponential fit is shown. For each boxplot, the central line is the median, edges of the box are 25th and 75th percentiles and the dotted line extends to the 5th and 95th percentiles. The mean is indicated by black dots.

ACPD
12, 4541–4588, 2012

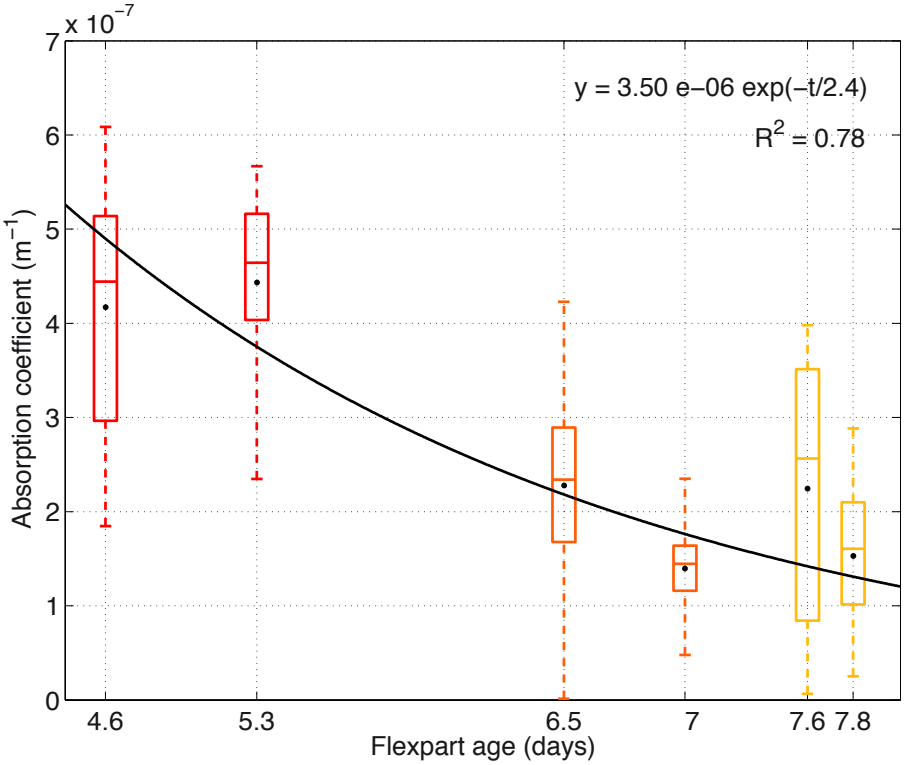

Fig. 7b. Evolution of the light absorption coefficient derived from PSAP measurements as a function of FLEXPART age. An exponential fit is shown in black.

ACPD
12, 4541–4588, 2012

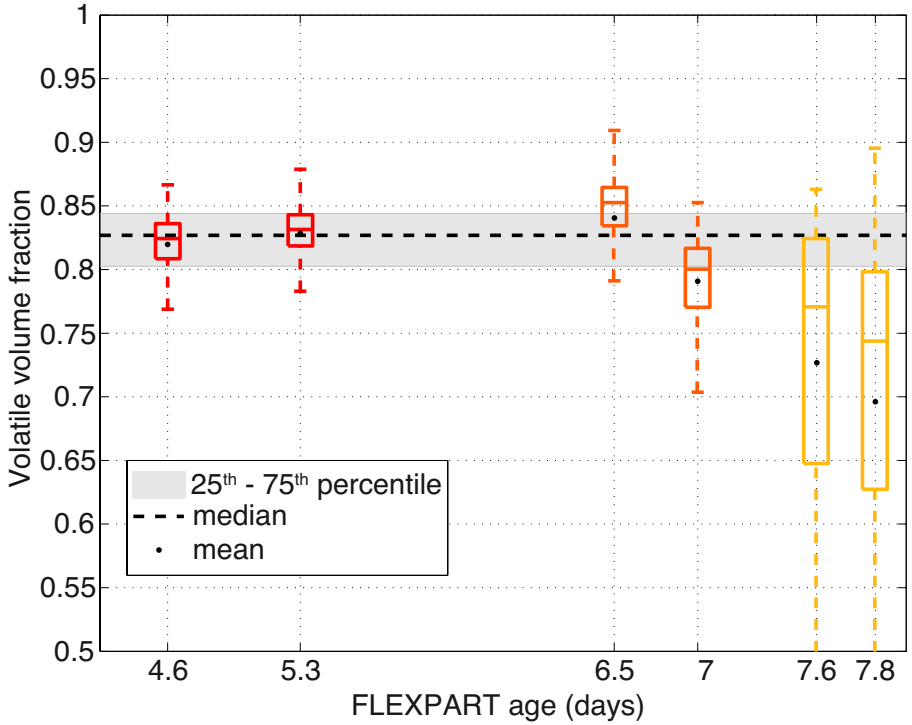

Fig. 7c. Presentation of aerosol $F_{volatile}$ as a function of the FLEXPART derived age of air masses. The mean volatile volume fraction for the 6 flight segments is plotted in black.

ACPD
12, 4541–4588, 2012

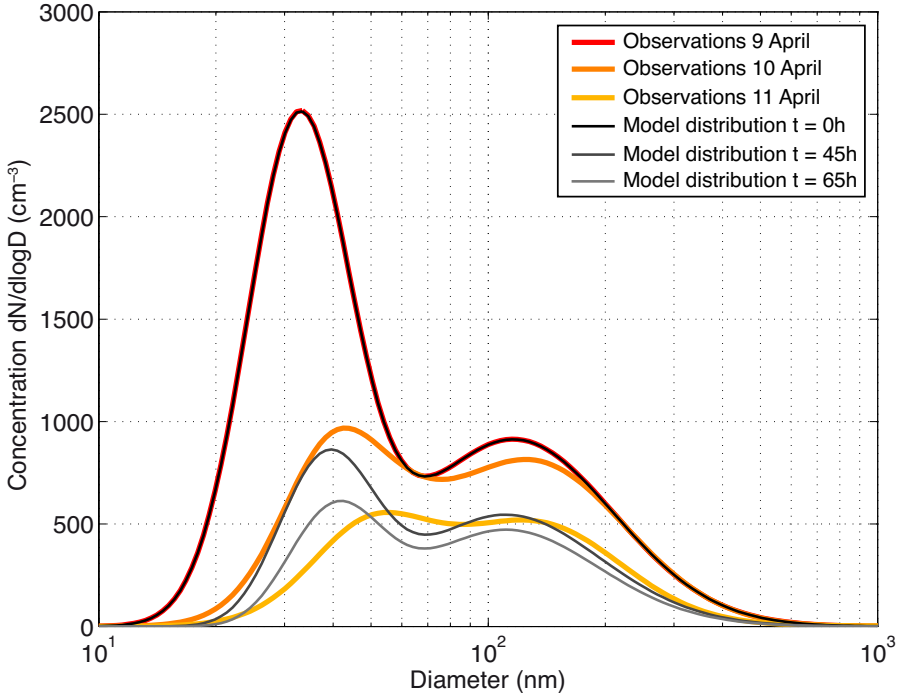

Fig. 8. Aerosol number size distributions observed (coloured lines) and simulated with a coagulation model (grey level lines) for flights on 9, 10 and 11 April. $t = 0$ corresponds to the mean FLEXPART age for the measurements of the plume on 9 April. See text for details.

ACPD
12, 4541–4588, 2012

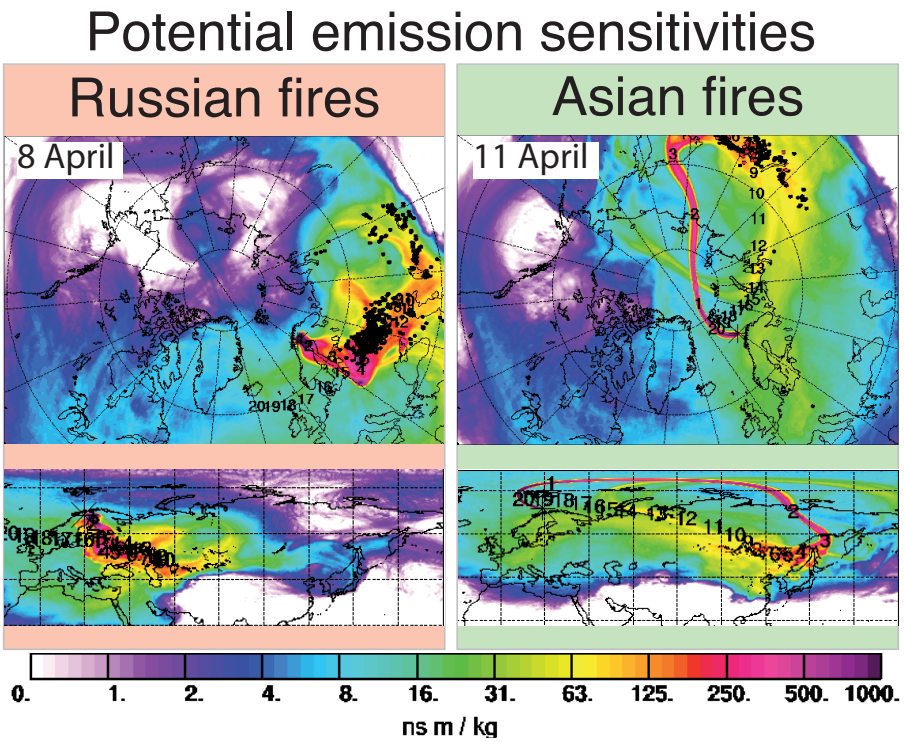

Fig. 9. FLEXPART column-integrated potential emission sensitivities for Russian (left) and Asian (right) forest fire plumes. Black and red dots represent agricultural and forest fires, respectively.

ACPD
12, 4541–4588, 2012

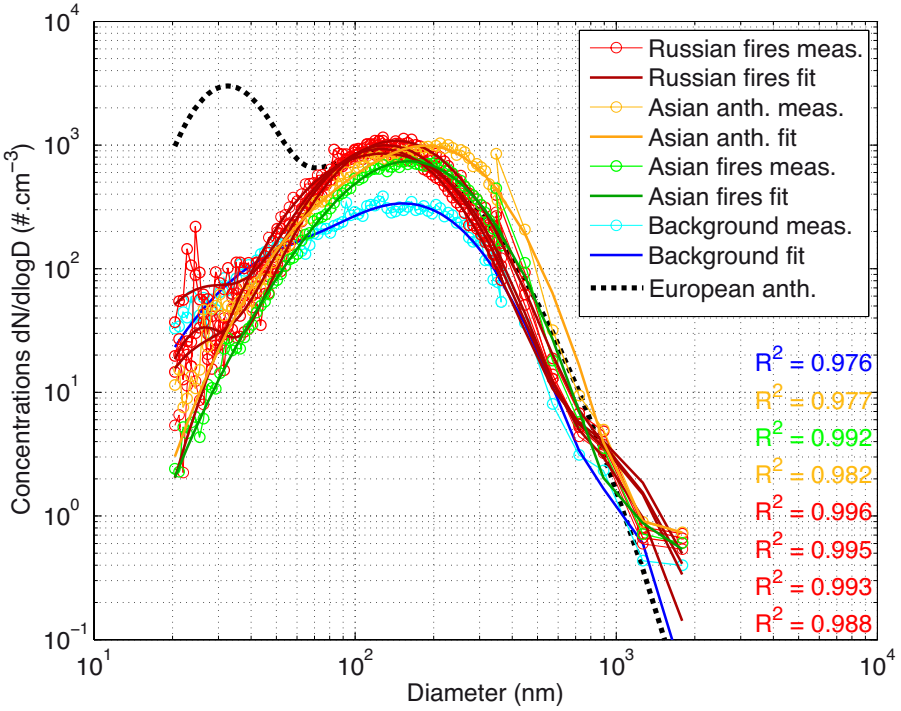

Fig. 10. Measured (thin solid line with circles) and fitted (thick solid line) aerosol number size distributions corresponding to Russian and Asian plumes transported to the Arctic. Distributions are fitted with three mode, corresponding correlation factors are indicated. Red and green distributions represent Russian and Asian forest fires, respectively; yellow distributions represent the Asian anthropogenic plume. For comparison reason, a polar background distribution is shown in blue and in addition, a distribution related to the European anthropogenic plume sampled on April 9th (discussed in the first case study).

ACPD
12, 4541–4588, 2012

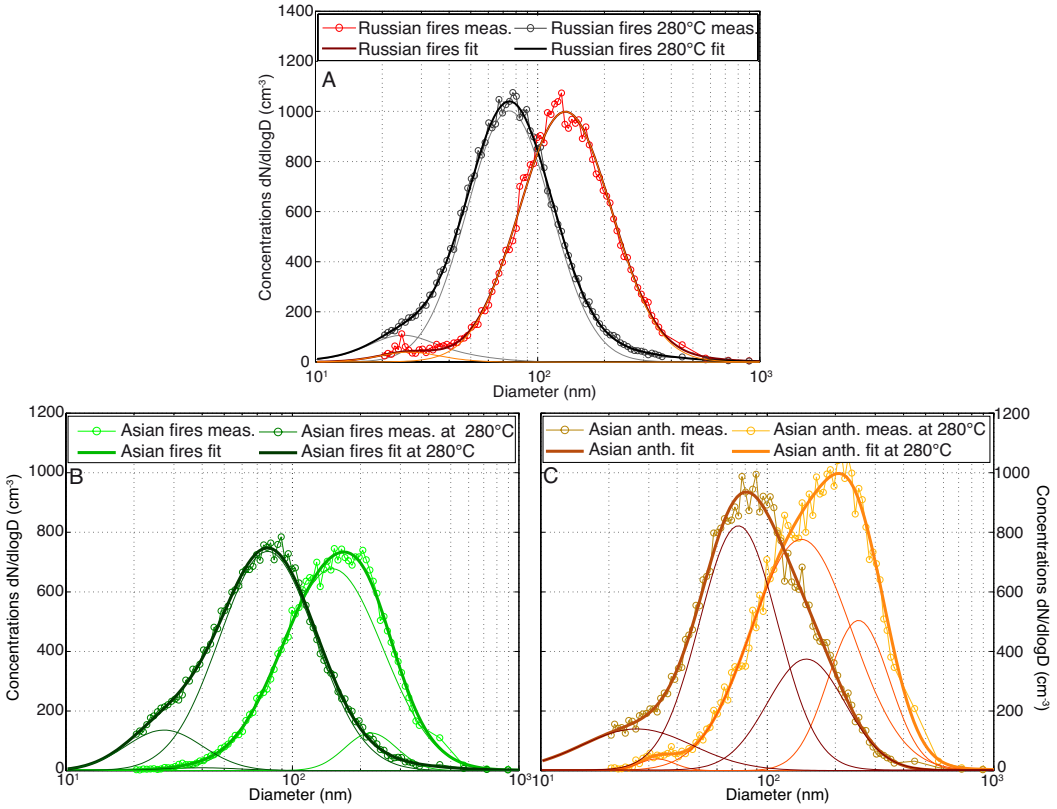

Fig. 11. Ambient and 280 ˚C aerosol number size distributions for **(a)** Russian fires air masses and **(b)** Asian fire and **(c)** Asian anthropogenic air masses.

ACPD
12, 4541–4588, 2012

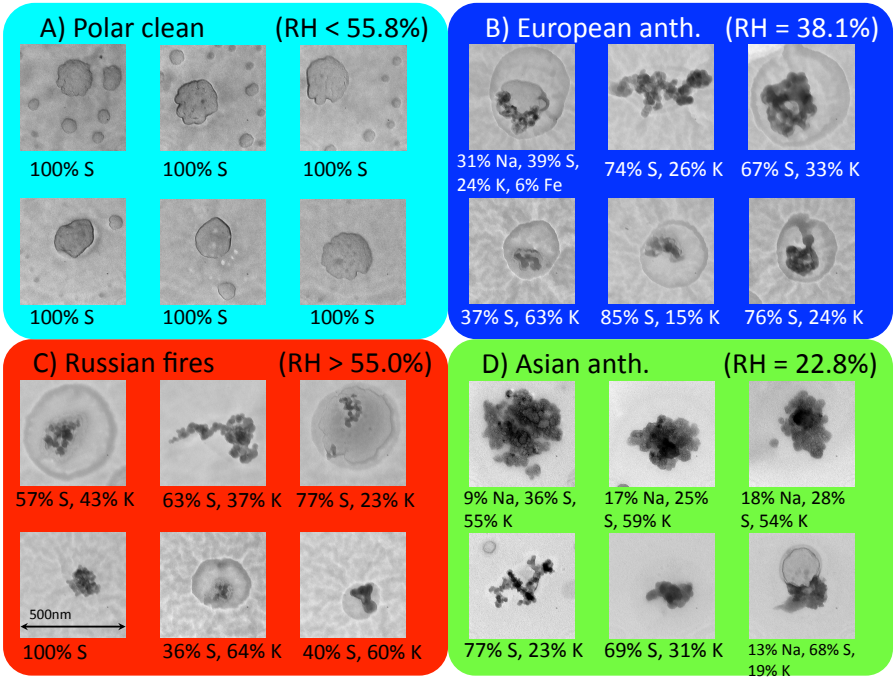

Fig. 12. Representative images of submicron aerosol particles sampled in-situ during POLARCAT flights. Particle origins are: Polar clean air **(A)**, European anthropogenic **(B)**, Russian fires **(C)** and Asian anthropogenic **(D)**. Width of images corresponds to 500 nm. Elemental compositions of particles, determined by EDX, are indicated in term of atomic ratio (C, N, O are excluded). See text for details.

ACPD
12, 4541–4588, 2012

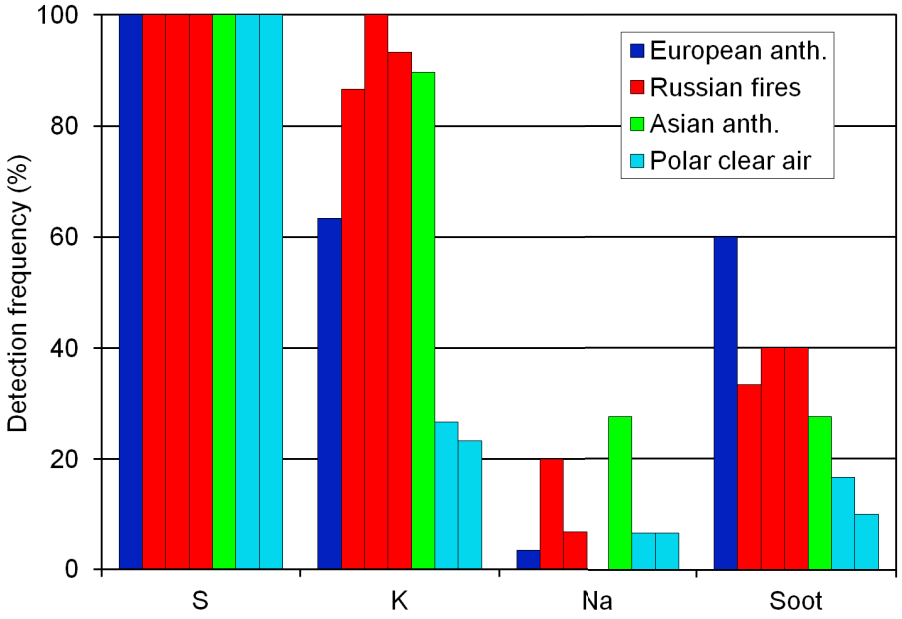

Fig. 13a. Detection frequency of the major elements (EDX) and soot (visual identification) among individual submicron aerosol particles.

ACPD
12, 4541–4588, 2012

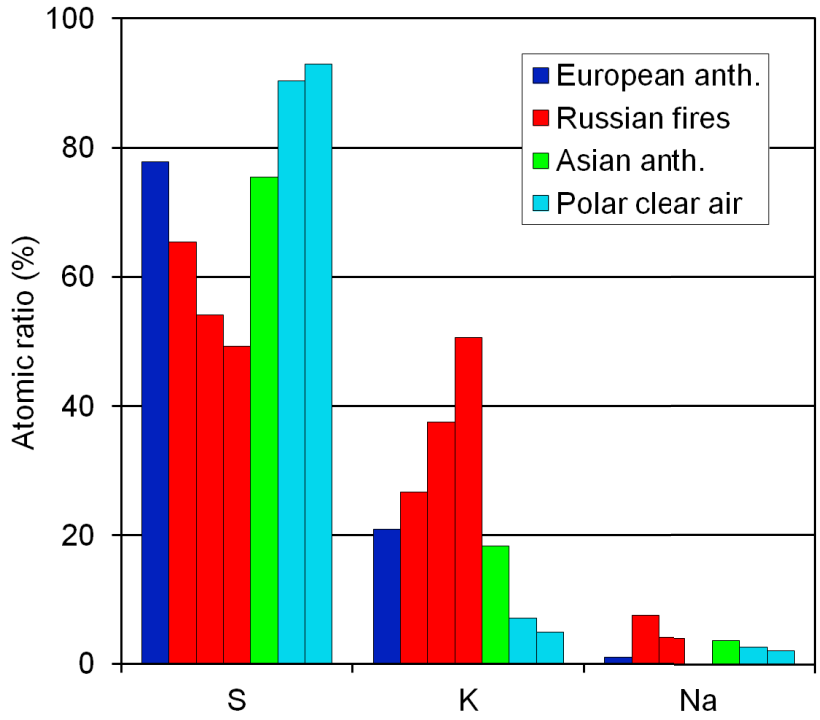

Fig. 13b. Atomic ratio of the major elements (EDX) among individual submicron aerosol particles.

ACPD
12, 4541–4588, 2012